Thermoplasmonics modeling: A Green's function approach

Guillaume Baffou,[1,*] Romain Quidant,[1,2] and Christian Girard[3]

[1]*ICFO, Institut de Ciencies Fotoniques, Mediterranean Technology Park, 08860 Castelldefels (Barcelona), Spain*
[2]*ICREA, Institució Catalana de Recerca i Estudis Avançats, 08010 Barcelona, Spain*
[3]*CEMES, CNRS–Université Paul Sabatier, 29 rue J. Marvig, F-31005 Toulouse, France*

We extend the discrete dipole approximation (DDA) and the Green's dyadic tensor (GDT) methods—previously dedicated to all-optical simulations—to investigate the thermodynamics of illuminated plasmonic nanostructures. This extension is based on the use of the thermal Green's function and a original algorithm that we named *Laplace matrix inversion*. It allows for the computation of the steady-state temperature distribution throughout plasmonic systems. This hybrid photothermal numerical method is suited to investigate arbitrarily complex structures. It can take into account the presence of a dielectric planar substrate and is simple to implement in any DDA or GDT code. Using this numerical framework, different applications are discussed such as thermal collective effects in nanoparticles assembly, the influence of a substrate on the temperature distribution and the heat generation in a plasmonic nanoantenna. This numerical approach appears particularly suited for new applications in physics, chemistry, and biology such as plasmon-induced nanochemistry and catalysis, nanofluidics, photothermal cancer therapy, or phase-transition control at the nanoscale.

PACS number(s): 65.80.−g, 73.20.Mf, 41.20.Cv, 44.05.+e

Nanoscale control of temperature appears as one of the most challenging aspect of Nanotechnologies. The ability to design and measure a temperature distribution at the nanoscale may lead to novel and significant developments in physics, chemistry, and biology. Until now, this research area remains mostly unexplored, mainly because of the diffusive nature of heat that makes it difficult to investigate experimentally with any noninvasive far-field approach. Opposingly, research in nano-optics and nanophotonics are much more advanced precisely because of the possible propagative nature of light.

Recently, new experimental photothermal approaches have been developed, which triggered a new gain of interest in the field of nanothermodynamics: first, the use of plasmonic nanoparticles,[1–5] they could be the basis components of sophisticated temperature-control nanodevices since they act as ideal confined nanosources of heat, remotely controllable by light.[6,7] Then, original optical experimental techniques, based on optical index variation in the surroundings[8] or fluorescence polarization anisotropy,[9,10] demonstrate different capabilities to investigate the heat generation and map the temperature with a subwavelength resolution. These two techniques, based on optical far-field measurements, have been used to unravel intricate nanoscale thermal processes, especially when related to plasmonic nanoparticles. To support this recent experimental development in nanotechnology, understand the underlying physics, and predict new nanothermodynamics-related phenomena, new numerical approaches coupling optics and thermodynamics have to be formulated.

In this paper, we propose a unified formalism to model a large class of experimental systems composed of metallic nanostructures where photothermal effects occur. The formalism consists of further extending both the discrete dipole approximation (DDA) and Green's dyadic tensor (GDT) methods—previously devoted to electrodynamic simulations—to the description of photoinduced thermal effects, and, in particular, to compute temperature profiles. In the same spirit of DDA and GDT methods, the thermal extension we developed is also based on a Green's function formalism. This paper is divided in two sections.

The first section is dedicated to the DDA method and its thermal extension. To illustrate this approach, well suited to address problems involving colloidal nanoparticles, we investigate the heat generation and temperature distribution around nanoparticles deposited on a glass substrate. We discuss the influence of the solvent and the substrate on the expected temperature increase, as well as the physics of heat generation throughout nanoparticles arrays.

The second section is dedicated to the thermal extension of the GDT method, suited for more complex geometries. This approach turns out to be nontrivial since it requires the computation of a fictive heat generation density inside the metallic structure. The associated algorithm that we named *Laplace matrix inversion* (LMI) is explained in detail. As a direct application, we discuss the temperature profile generated around a plasmonic nanoantenna, which we compare with the optical near-field distribution.

Some additional questions that our numerical approach may raise are gathered in two appendices. They concern the influence of any interface thermal resistance (Appendix A) and thermoinduced fluid convection (Appendix B) on the actual steady-state temperature field distribution.

I. OPTOTHERMAL DISCRETE DIPOLE APPROXIMATION

A. Discrete dipole approximation

The DDA is a general method to investigate the optical properties of nanoparticles assembly.[11,12] It can be used to compute absorption and scattering cross sections, optical near-field, or light-radiation diagram. DDA is particularly suited to take into account the presence of a planar interface between two dielectric media to model for example the presence of a substrate. Such a typical system is represented schematically in Figs. 1.
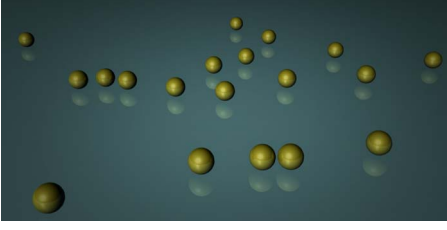
FIG. 1. (Color online) Assembly of gold nanoparticles deposited on a glass substrate, which represents one of the typical systems that the DDA method can investigate.

In the following, the particles are assumed dielectric but not magnetic (magnetic permittivity $\mu = \mu_0$). The size of the particle is supposed to be small compared to the wavelength of the incoming light. The electric permittivity and the polarizability of the particles are assumed isotropic to simplify the derivations. However, extension to arbitrary dielectric tensor or ellipsoidal particles is also permitted.

Consider N identical dipolar spherical particles of radius a, polarizability α at the positions $\mathbf{r}_i$ and an incident monochromatic light characterized by a complex electric-field amplitude $\mathbf{E}_0(\mathbf{r}, \omega)$. The polarization amplitude $\mathbf{p}_i(\omega)$ of the nanoparticle i is

$$\mathbf{p}_i = \alpha(\omega)\mathbf{E}_i^{\text{ext}}(\omega) \tag{1}$$

$\mathbf{E}_i^{\text{ext}}(\omega)$ is the external electric field amplitude experienced by the particle i. It has two origins: the incident field $\mathbf{E}_0(\mathbf{r}_i, \omega)$ and the field radiated by the $N-1$ neighbor particles. Henceforth the ω dependency will be omitted in the equations for the sake of clarity. In the dipolar approximation, the polarizability of the particle reads

$$\alpha = \frac{\alpha_0}{1 - (2/3)ik^3\alpha_0}, \tag{2}$$

where

$$\alpha_0 = 4\pi\varepsilon_0 a^3 \frac{\varepsilon - \varepsilon_{\text{m}}}{\varepsilon + 2\varepsilon_{\text{m}}}, \tag{3}$$

where ε and ε_{m} are the electric permittivities of the nanoparticle and the surrounding medium, respectively. Formula (2) stands for a correction to the standard Clausius-Mossotti polarizability α_0. This correction is required to verify the optical theorem and energy conservation but can be neglected for small particles, typically less than 20 nm in diameter.

Note that in nanoplasmonics, the use of the bulk permittivity ε is *a priori* not straightforward since the electron mean free path is only 50 nm in gold. Some surface effects could be expected additionally to the electron-phonon interaction (Joule effect) occurring in volume and responsible for the temperature increase. However, it has been shown experimentally, in particular by Link and El-Sayed[13] and by Hartland *et al.*,[14] that no size dependence of the electron-electron and electron-phonon relaxations exists in gold nanoparticles down to at least 9 nm in diameter. This is due to the elastic scattering of electrons by the particle surface, which does not lead to any energy transfer from electrons to surface phonons. For this reason the use of the bulk permittivity is

usually sufficient and justified to describe the physical properties of gold nanoparticles.

The problem consists in calculating the electric field amplitudes $\mathbf{E}_i^{\text{ext}}$ at each particle position i. Since all the particles are in interaction with each other, this problem is self-consistent. The use of the Green's dyadic tensor formalism is appropriate to simply express and formally solve the problem. The equations read[11,15]

$$\mathbf{E}_i^{\text{ext}} = \mathbf{E}_0(\mathbf{r}_i) + \sum_{j \neq i} \mathbb{S}(\mathbf{r}_i, \mathbf{r}_j) \cdot \mathbf{p}_j \tag{4}$$

and can be recast using Eq. (1)

$$\mathbf{E}_i^{\text{ext}} = \mathbf{E}_0(\mathbf{r}_i) + \sum_{j \neq i} \alpha\mathbb{S}(\mathbf{r}_i, \mathbf{r}_j) \cdot \mathbf{E}_j^{\text{ext}}, \tag{5}$$

where $\mathbb{S}(\mathbf{r}_i, \mathbf{r}_j)$ is the electric field propagator (also called Green's dyadic tensor) associated to the surroundings. The self-consistency is evidenced by Eq. (5). The Dyson method allows for recasting Eq. (5) into a resolved form where the self-consistency is removed[11,15]

$$\mathbf{E}_i^{\text{ext}} = \mathbf{E}_0(\mathbf{r}_i) + \sum_{j \neq i} \alpha\mathbb{K}(\mathbf{r}_i, \mathbf{r}_j) \cdot \mathbf{E}_0(\mathbf{r}_j), \tag{6}$$

where $\mathbb{K}(\mathbf{r}_i, \mathbf{r}_j)$ is the Green dyadic function of the complete system (particles plus surrounding surface). The central part of the algorithm consists in calculating the generalized propagators $\mathbb{K}(\mathbf{r}_i, \mathbf{r}_j)$, which can be done by N successive inversions of 3×3 matrices. Once the electric field amplitude $\mathbf{E}_i^{\text{ext}}$ is known at each position $\mathbf{r}_i$, it can be calculated at any position $\mathbf{r}$ using the electric field propagator

$$\mathbf{E}(\mathbf{r}) = \mathbf{E}_0(\mathbf{r}) + \sum_{j=1}^{N} \alpha\mathbb{S}(\mathbf{r}, \mathbf{r}_j) \cdot \mathbf{E}_j^{\text{ext}}. \tag{7}$$

B. Calculation of the thermal field

We now explain how the steady-state temperature distribution can be obtained from the knowledge of the electric field distribution $\mathbf{E}_i^{\text{ext}}$ calculated in the previous paragraph. From now on, the temperature T has to be understood as a temperature increase above the ambient temperature. In a steady-state regime, the temperature profile $T(\mathbf{r})$ throughout the system is solution of the Poisson equation

$$\kappa\nabla^2 T(\mathbf{r}) = -q(\mathbf{r}), \tag{8}$$

where κ is the thermal conductivity of the medium at $\mathbf{r}$. The thermal conductivities of all the media are supposed homogeneous and isotropic. $q(\mathbf{r})$ is the heat source density. Due to light absorption, the particles are the sources of heat of the problem. For a single particle, the light absorption cross section reads

$$\sigma_{\text{abs}} = \frac{k}{4\pi\varepsilon_0}\text{Im}(\alpha) - \frac{2}{3}\frac{k^4}{(4\pi\varepsilon_0)^2}|\alpha|^2. \tag{9}$$

The second term is usually negligible for small particles. The heat power Q_i delivered by a particle i is

$$Q_i = \sigma_{\mathrm{abs}} n \frac{c \varepsilon_0}{2} |\mathbf{E}_i^{\mathrm{ext}}|^2, \tag{10}$$

where n is the optical index of the surrounding medium.

Let us consider first the case of a single isolated spherical nanoparticle ($N=1$) at the position $\mathbf{r}_i$ in a homogeneous medium of the thermal conductivity κ. Since no heat source is present in the medium surrounding the nanoparticle, the temperature distribution outside the nanoparticle can be determined from the Laplace equation

$$\nabla^2 T(\mathbf{r}) = 0. \tag{11}$$

The problem can be solved analytically and easily in spherical coordinates and yields

$$T(\mathbf{r}) = T_0 \frac{a}{|\mathbf{r} - \mathbf{r}_i|} \quad \text{for} \quad |\mathbf{r} - \mathbf{r}_i| \geq a. \tag{12}$$

In the following, we will suppose that the thermal conductivity of the nanoparticle is much higher than the one of the surrounding medium. This approximation is usually very good for metallic nanoparticles in a dielectric environment such as water or glass. In this case, the temperature can be considered as uniform inside the nanoparticle

$$T(\mathbf{r}) = T_0 \quad \text{for} \quad |\mathbf{r} - \mathbf{r}_i| \leq a. \tag{13}$$

The particle temperature T_0 can be retrieved by writing an energy conservation equation. The power going through the particle interface must equal the heat power Q delivered by the particle

$$Q = \int_S - \kappa \nabla T(\mathbf{r}) \cdot \mathbf{dS}, \tag{14}$$

which naturally yields

$$T_0 = \frac{Q}{4\pi\kappa a} \tag{15}$$

and

$$T(\mathbf{r}) = \frac{Q}{4\pi\kappa|\mathbf{r} - \mathbf{r}_i|} \quad \text{for} \quad |\mathbf{r} - \mathbf{r}_i| \geq a. \tag{16}$$

Note that formula (16) involves the scalar Green's function $G(\mathbf{r}, \mathbf{r}_i)$ (that vanishes at the infinity) associated to the Poisson Eq. (8) and a Dirac source distribution $\delta(\mathbf{r} - \mathbf{r}_i)$ in an infinite homogeneous medium

$$G(\mathbf{r}, \mathbf{r}_i) = \frac{1}{4\pi\kappa|\mathbf{r} - \mathbf{r}_i|}. \tag{17}$$

Interestingly, it has been recently reported that the thermal energy transfer between a plasmonic nanoparticle and a surrounding liquid can be affected by a molecular coating on the nanoparticle surface since acting as a surface thermal resistance.[16] This effect is not taken into account in our method, but we show in Appendix A that, while the nanoparticle inner temperature can be indeed modified, a thermal surface resistance does not change the temperature profile in the surrounding medium, which is what usually matters while investigating thermoinduced phenomena.
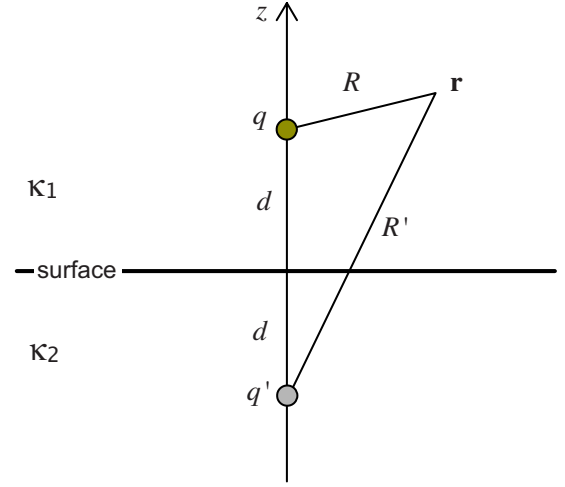

FIG. 2. (Color online) The temperature distribution originating from a heat source q facing a surface can be derived by the image method usually used in electrostatics.

Another effect that could modify and distort the calculated temperature distribution around plasmonic structures is a possible thermoinduced fluid convection, similar to the Marangoni effect.[17] We show in Appendix B that any thermoinduced fluid motion has no influence regarding the temperature profile for usual temperature increase and length scales in plasmonics.

Let us consider now the presence of a planar interface separating two infinite media 1 and 2 [Fig. 2]. The first infinite medium has a thermal conductivity κ_1 and contains the particle and the second one has a thermal conductivity κ_2 and can stand for a glass substrate. We consider an arbitrary distance d between the center of the spheric particle and the interface. The problem consisting in calculating the temperature profile is formally equivalent to the electrostatic problem consisting in calculating the electric potential distribution created by a charge facing an interface between two dielectric media. This problem can be solved using the image method.[18] In this analogy, the temperature is equivalent to the electric potential and the thermal conductivity is equivalent to the electric permittivity. The thermal Green's function now reads

$$G(\mathbf{r}, \mathbf{r}_i) = \frac{1}{4\pi\kappa_1} \left[\frac{1}{R} + \left(\frac{\kappa_2 - \kappa_1}{\kappa_2 + \kappa_1} \right) \frac{1}{R'} \right] \quad \text{for} \quad z \geq 0,$$

$$G(\mathbf{r}, \mathbf{r}_i) = \frac{1}{4\pi\kappa_2} \frac{1}{R} \left(\frac{2\kappa_2}{\kappa_2 + \kappa_1} \right) \quad \text{for} \quad z \leq 0, \tag{18}$$

where

$$R = \sqrt{(x - x_i)^2 + (y - y_i)^2 + (z - d)^2},$$

$$R' = \sqrt{(x - x_i)^2 + (y - y_i)^2 + (z + d)^2}.$$

Then, the temperature profile is simply given by

$$T(\mathbf{r}) = G(\mathbf{r}, \mathbf{r}_i) Q. \tag{19}$$

Let us consider now the case of an assembly of metallic particles under illumination. At any position **r** of the medium, the temperature $T(\mathbf{r})$ is given by a linear superposition

$$T(\mathbf{r}) = \sum_{j=1}^{N} G(\mathbf{r}, \mathbf{r}_j) Q_j, \qquad (20)$$

where $G(\mathbf{r}, \mathbf{r}_i)$ is the Green's function associated to the system that is given by formula (17) if the particles are in a homogeneous medium or by formula (18) if there is an interface separating two different media.

Then, the inner temperature T_i of each particle can be retrieved this way

$$T_i = \sum_{j=1}^{N} G(\mathbf{r}_i, \mathbf{r}_j) Q_j, \qquad (21)$$

where $G(\mathbf{r}_i, \mathbf{r}_i) = 1/(4\pi\kappa a)$ accordingly to Eq. (15).

C. Applications

1. Influence of the surrounding media

In this paragraph, we focus on the influence of a substrate and a solvent on the temperature increase and temperature profile around plasmonic nanoparticles. We consider a chain of 10 gold spheres, 15 nm in diameter, separated by 2 nm gaps the one from each other. We consider three successive configurations: an homogeneous medium, a glass substrate in air, and glass substrate in water. The thermal conductivities of air, water and glass are, respectively, 0.025 W/m K, 0.6 W/m K, and 0.9 W/m K. Optical simulations have been performed using the regular DDA approach to compute the power delivered by each nanoparticle. Then, the temperature profile has been calculated using the thermal DDA extension. Figure 3 displays side views of the temperature profile around the plasmonic chain in various environments. The distance between the chain and the substrate is also artificially varied [Figs. 3(d) and 3(f)] to underline the importance of the vicinity of an interface with a conductive medium on the heat release.

In a homogeneous medium, the temperature profile (up to a constant prefactor) is independent of the medium conductivity. In other words, the typical temperature decay length in the surrounding medium is not dependent on the medium conductivity. Such a behavior can be observed in comparing Figs. 3(a) and 3(b): the two temperature distributions and decay lengths look the same even though the medium conductivity is very different. This general rule comes from the fact that the temperature distribution around the plasmonic structure is governed by the Laplace equation: $\nabla^2 T(\mathbf{r}) = 0$ in which the thermal conductivity no longer appears.

However, when the medium is not unique and infinite, the temperature profile does depend on the relative conductivities of the different media. For a glass substrate in air [Figs. 3(c) and 3(d)], the vicinity of the surface substantially helps to release the heat and tends to lower the nanoparticles temperature. For a glass substrate in water [Figs. 3(e) and 3(f)], the overall temperature is lower compared to the previous case since water contributes to a better heat diffusion than
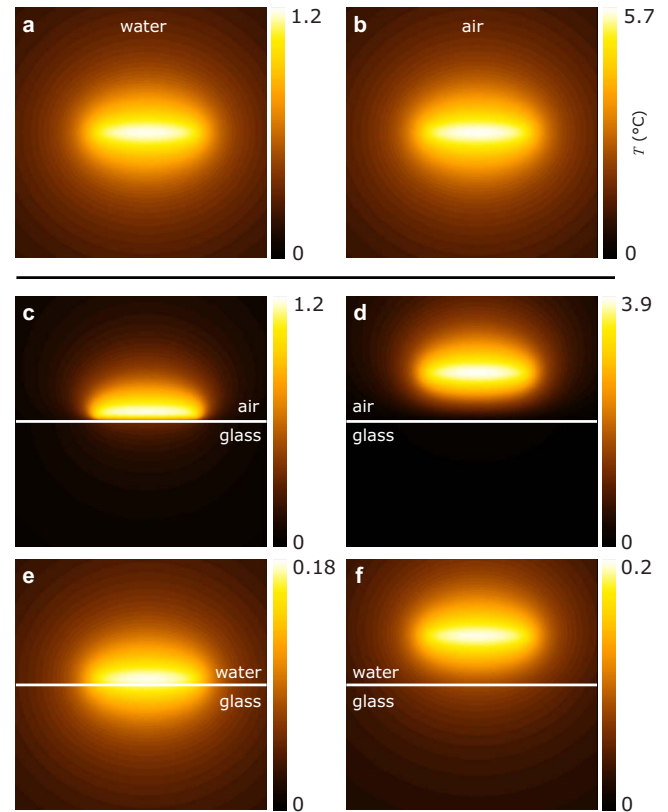

FIG. 3. (Color online) Side view of the temperature map of a chain of ten particles 15 nm in diameter and separated by 2 nm the one from each other. The structure is shined form the bottom ($\lambda = 600$ nm, $P = 10$ mW/μm^2) with a polarization along the nanoparticle chain.

air. The general trend to keep in mind is: the higher the thermal conductivity, the lower the temperature of the structure.

2. Collective effects

In this paragraph, we study the temperature increase within an array of $N \times N$ particles as a function of N. The nanoparticles are lying upon glass and immersed in water. Such a system can be used in thermoplasmonics for catalysis or biological applications. The question is to know what temperature dependence can be expected as a function of the illumination area and if some co-operative effects can be seen.[19]

Figure 4(b) displays the temperature increase calculated in the center of an array of $N \times N$ particles as a function of N. The nanoparticles are immersed in water, lying upon a glass substrate and illuminated at $\lambda = 530$ nm. A linear dependence is clearly observed. As a consequence, when a regular two-dimensional nanoparticle array is illuminated by a circular beam of a given power, the temperature increase within the nanoparticle array is proportional to the beam diameter $2R$ for a given illuminance I_0 and inversely proportional to the beam diameter for a given power $P_0 = \pi R^2 I$. Experimentally, the first case corresponds to an illuminating beam, whose diameter R is set by an iris; The second case corresponds to
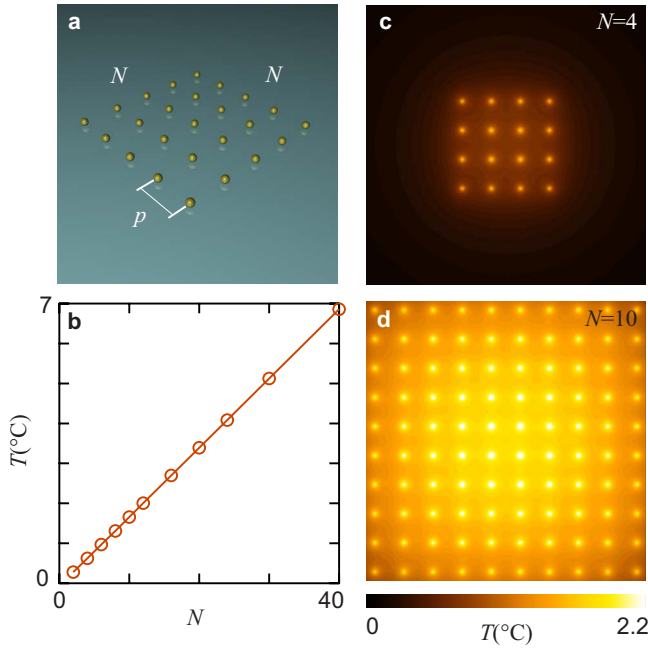
FIG. 4. (Color online) Numerical simulations regarding a $N \times N$ array of plasmonic nanoparticles lying upon glass, 40 nm in diameter, $p=300$ nm in pitch. The structure is shined from the bottom ($\lambda=520$ nm, $P=1$ mW/μm^2). (a) three-dimensional (3D) representation of the system (for $N=5$). (b) Temperature in the center of the array as a function of the size of the array showing a linear dependence. (c) Temperature map over an array of $N^2=4\times4$ cells. (d) Temperature map over an array of $N^2=10\times10$ cells.

an illuminating beam, whose diameter R is changed by unfocusing the beam.

II. OPTOTHERMAL GREEN'S DYADIC TENSOR METHOD

A. Green's dyadic tensor method

The GDT method is suited to compute the electromagnetic field inside and outside particles of arbitrarily complex geometry, in the possible presence of a planar interface separating two homogeneous media. The basic idea is to gather the previous dipoles considered in the DDA to form a volume (Fig. 5). However, an important point has to be stressed: these dipoles *no longer* represent physical spheres. In the GDT approach, the mesh has to be thought as an assembly of coordinates $\mathbf{r}_i$, where localized dipoles are located. This is a way to discretize the polarization field of the structure.

The numerical frameworks of GDT and DDA are very similar since a self consistent assembly a *dipoles* has to be considered in both cases. This is why DDA and GDT are often assimilated or presented in parallel although the natures of the numerical systems are different: in the DDA case, the dipoles represent spheres and are endowed with the sphere polarizability [Eq. (2)], while in the present GDT case, the dipoles are endowed with the bulk susceptibility of the metal $\chi(\omega)$

$$\chi = \varepsilon - \varepsilon_m \quad (22)$$

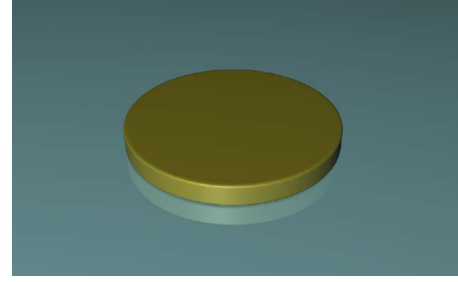times the volume of the unit cell v.

FIG. 5. (Color online) The Green's dyadic tensor technique enables one to model arbitrarily large non-spherical objects, type lithographic nanostructures. The meshing of the system is restricted to the nanostructure itself. This figure represents a typical system and geometry.

The second difference with DDA appears in the sum of Eq. (5) where a nonzero depolarization term has to be taken into account for $i=j$

$$\mathbb{S}(\mathbf{r}_i, \mathbf{r}_i) = -\frac{1}{3\varepsilon_m v}\mathbb{I}, \quad (23)$$

where v is the volume of a unit cell of the structure meshing and $\mathbb{I}$ the identity matrix. In the case of a compact meshing—either fcc or hcp—the unit-cell volume is $v=(2a)^3/\sqrt{2}$.

The previous DDA self-consistent Eq. (5) reads thus now in the GDT approach

$$\mathbf{E}_i = \mathbf{E}_0(\mathbf{r}_i) + \sum_{j=1}^{N} v\chi\mathbb{S}(\mathbf{r}_i, \mathbf{r}_j) \cdot \mathbf{E}_j. \quad (24)$$

B. Calculation of the thermal field

The heat power arising from each cell of the structure reads

$$Q_i = \omega v \, \mathrm{Im}(\varepsilon)|\mathbf{E}_i|^2. \quad (25)$$

Since we are now investigating an extended structure, we can define a continuous heat source density $q(\mathbf{r})$ inside the structure as the heat power Q_i divided by the volume of a cell

$$q(\mathbf{r}_i) = \omega \, \mathrm{Im}(\varepsilon)|\mathbf{E}_i|^2. \quad (26)$$

In the GDT Method, we cannot directly use DDA Eqs. (20) and (21) to calculate the temperature distribution. The situation is indeed different since the dipoles belong now to the same piece of metal while they stand for isolated metal spheres in the DDA case. The cells are thus now interacting with each other also through the thermal conductivity of the metal structure. The direct consequence of the internal heat diffusion is known: it tends to make the temperature profile uniform.[6,7] Simply using DDA amounts to suppressing this internal temperature diffusion and leads indeed to a nonuniform temperature profile inside the structure as represented in Fig. 6(b), which does not correspond to reality. The original approach we are developing in the following basically consists in using DDA [Eq. (21)] but with a fictive heat source density that imposes a uniform temperature field.
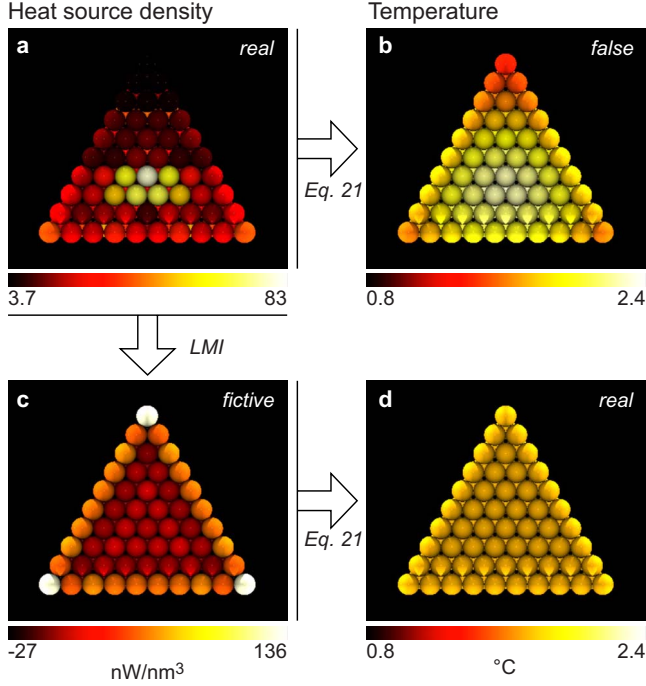
FIG. 6. (Color online) Explanation of the LMI method based on the top view of a triangular plasmonic structure. The hexagonal mesh of the structure has been represented as an assembly of packed spheres. (a) Heat source density distribution $q_i = \omega v \, \mathrm{Im}(\varepsilon)|\mathbf{E}_i|^2$ calculated in a triangular gold nanostructure under illumination. (b) Internal temperature T_i calculated from the heat source density q_i of figure a using Eq. (21). This procedure is valid in DDA but gives a wrong temperature distribution in GDT since non uniform. (c) Fictive heat source density distribution associated to a fictive internal electric field $\mathbf{e}_i$, obtained by the LMI method. (d) Real temperature profile, that is indeed uniform, inside the plasmonic structure obtained from the fictive heat source density distribution of figure c by using Eq. (21).

Start from the DDA Eq. (21) giving the temperatures T_i in each cell. Using Eq. (10) this equation can be recast into a matrix formulation linking the temperature and the square electric field amplitude

$$T_i = \frac{\omega v \, \mathrm{Im}(\varepsilon)}{4\pi\kappa} \sum_{j=1}^{N} \mathbb{A}_{ij} |\mathbf{E}_j|^2. \tag{27}$$

Equation (27) has to be seen as a matricial equation linking the vectors $(T_i)_{i\in[1,N]}$ and $(|\mathbf{E}_i|^2)_{i\in[1,N]}$. Let us call $\mathbb{A}$ the *Laplace matrix*. According to Eq. (17), in an infinite homogeneous medium the Laplace matrix elements of $\mathbb{A}$ read

$$\mathbb{A}_{ij} = \frac{1}{|\mathbf{r}_i - \mathbf{r}_j|} \tag{28}$$

while according to Eq. (18), in the presence of a surface, the Laplace matrix elements of $\mathbb{A}$ read

$$\mathbb{A}_{ij} = \frac{1}{|\mathbf{r}_i - \mathbf{r}_j|} - \frac{\kappa_2 - \kappa_1}{\kappa_2 + \kappa_1} \frac{1}{|\mathbf{r}_i - \mathbf{r}_j^{\star}|}, \tag{29}$$

where $\mathbf{r}_j^{\star} \equiv (x_j, y_j, -z_j)$ is the image of $\mathbf{r}_j$ through the surface.

To work out the real temperature distribution, the technique we propose consists in calculating a fictive distribution $\mathbf{e}_j^2$ that results in a uniform temperature inside the metal structure. To do that, one just needs to invert the $N \times N$ Laplace matrix $\mathbb{A}$ and apply it to a uniform temperature distribution $T_i = T_0$

$$\mathbf{e}_i^2 = \frac{4\pi\kappa}{\omega v \, \mathrm{Im}(\varepsilon)} \sum_{j=1}^{N} (\mathbb{A}^{-1})_{ij} T_0. \tag{30}$$

Note that some source terms $\mathbf{e}_i^2$ can be negative. In this case they act as fictive heat wells.

Then, the unknown temperature T_0 can be obtained by energy conservation

$$\sum_{i=1}^{N} \mathbf{e}_i^2 = \sum_{i=1}^{N} |\mathbf{E}_i|^2. \tag{31}$$

Using Eqs. (25), one can derive one of the most important formula of this paper, which gives the steady-state temperature of a plasmonic structure under illumination

$$T_0 = \frac{Q}{4\pi\kappa \sum\limits_{i=1}^{N} \sum\limits_{j=1}^{N} (\mathbb{A}^{-1})_{ij}}. \tag{32}$$

Interestingly, by comparing Eqs. (15) and (32), it turns out that $\Sigma(\mathbb{A}^{-1})_{ij}$ appears as an effective radius of the nanostructure, which we shall name the Laplace radius r_{L}

$$r_{\mathrm{L}} = \sum_{i,j} (\mathbb{A}^{-1})_{ij}. \tag{33}$$

Equation (32) along with this concept of Laplace radius allows for the computation of the steady-state temperature of a plasmonic structure only from the knowledge of the absorbed power $Q = \sigma_{\mathrm{abs}} I$ and the Laplace matrix $\mathbb{A}$. This radius is easy to compute since the matrix elements of $\mathbb{A}$ only depend on the geometry and the meshing, no optical or thermal calculation is necessary. It just requires an $N \times N$ matrix inversion where N is the number of meshing cells. The nature of the meshing does not matter, it does yield to a good estimation of the Laplace radius as long as the meshing remains regular and refined enough.

Finally the temperature anywhere in the surroundings can be calculated using the regular Eq. (21) applied to the fictive heat source density distribution $q_i = \omega v \, \mathrm{Im}(\varepsilon) \mathbf{e}_i$

$$T(\mathbf{r}) = \sum_{j=1}^{N} G(\mathbf{r}, \mathbf{r}_j) \omega v \, \mathrm{Im}(\varepsilon) \mathbf{e}_i. \tag{34}$$

C. Validity of the Laplace matrix inversion method

The validity of the use of a fictive heat source density distribution is *a priori* not straightforward. Here are the arguments that validate this approach. (i) By construction of the fictive electric field distribution, all the cells of the nanoparticle are bound to feature the same temperature, which is the required situation. The boundary conditions (uniform
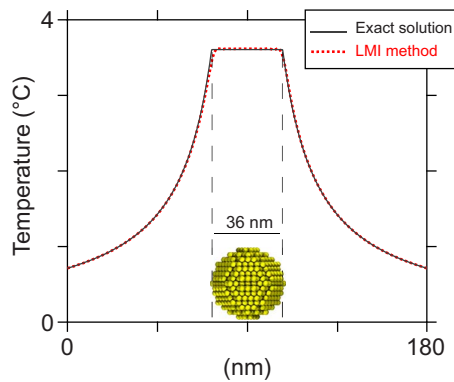
FIG. 7. (Color online) Temperature increase profile of a gold nanoparticle, 36 nm in diameter, under illumination (1 mW/μm^2, λ=530 nm). The Laplace matrix method using a fictive heat source density distribution shows a very good agreement with the analytical solution. The internal temperature of the particle is found to be 3.61 °C while the exact solution gives 3.56 °C.

temperature at the nanoparticle/medium interface) are then fulfilled. (ii) Outside the structure, the temperature field calculated using the LMI method and Eq. (34) is a solution of the Poisson equation since constructed as a linear superposition of thermal Green's functions.

From these two arguments, and given the unicity of the solution of a Laplace equation for given temperature boundary conditions (Dirichlet problem),[18] we can conclude that the temperature profile $T(\mathbf{r})$ obtained using this strategy is valid inside and outside the structure, up to a constant prefactor. Then, the energy conservation that we ensure in this formalism by Eq. (31) implies that the temperature distribution $T(\mathbf{r})$ that has the appropriate profile is also quantitatively valid.

As a visual example, we compute the temperature profile around a spherical gold nanosphere using this LMI method. We chose this geometry because it makes it possible to compare the numerical simulation with the exact analytical solution [Eq. (16)]. The results are presented in Fig. 7 and show a very good agreement even for a relatively low number of cells (N=1261 in this case). The computation gives a nanoparticle temperature of T_0=3.61 °C while this exact calculation gives T_0=3.56 °C. This small difference is due to the fact that the sphere diameter is not well defined due to the finite size of the mesh cell, which makes the interface slightly irregular. The effect can be minimized if need be by increasing the number of cells. Moreover, the calculated temperature profile outside the nanoparticle matches perfectly the analytical solution, which is a direct consequence of energy conservation.

Note that the Laplace matrix formalism that we propose in this paper is actually not restricted to plasmonics and thermodynamics. It stands for a general mathematical approach that can be applied to any problem relying on Laplace equation with a finite-size source domain featuring a uniform potential, such as in electrostatics or particle diffusion.
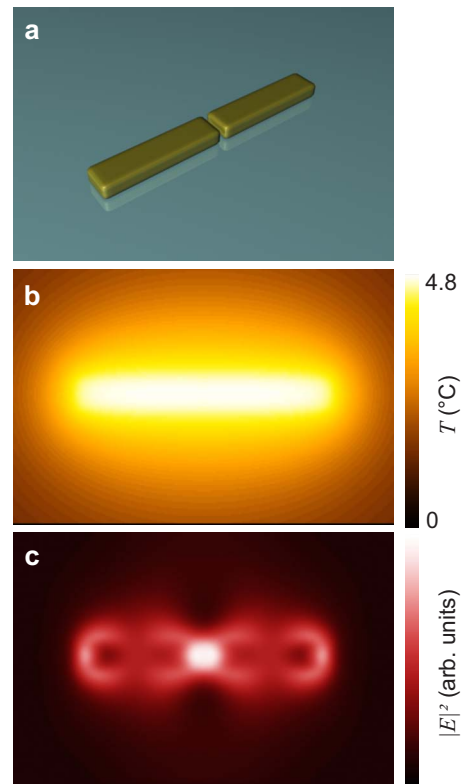

FIG. 8. (Color online) (a) 3D representation of a gap antenna. The two rods, 400 nm long, 100 nm wide, and 50 nm thick, are separated by a gap of 20 nm. The structure is lying upon a glass substrate and immersed in water. The structure is illuminated at the resonance wavelength λ=700 nm, P=1 mW/μm^2. (b) Top view of the temperature profile generated by the plasmonic structure calculated 10 nm above the structure. (c) Optical near-field profile calculated at the same height.

D. Application

1. Thermal versus optical near field

Originally, the GDT numerical approach, which the LMI method is based on, is suited for optical calculation. Hence, the GDT-LMI theoretical framework we present in this paper can be used easily to perform a systematic comparison between the optical near-field and the thermal near-field distributions around plasmonic structures under illumination.

To exemplify such an approach, we consider a gold gap-antenna structure.[20,21] This structure, as defined in Fig. 8, features a well-defined plasmonic resonance in the near infrared. We applied the GDT method to compute the optical near field and the LMI extension to compute the temperature profile surrounding such a structure. The optical near-field features a dramatic field enhancement in the gap region while the temperature profile is completely uniform throughout the structure. This illustrates the fact that, in plasmonics, gaps are suited to enhance the optical near field but are not especially favorable for heat generation.

As reported in a previous work,[9] the optimization of plasmonic structures as nanosources of light does not follow the same rules as the optimization as nanosources of heat. For this reason, such a systematic comparison will help unravel-
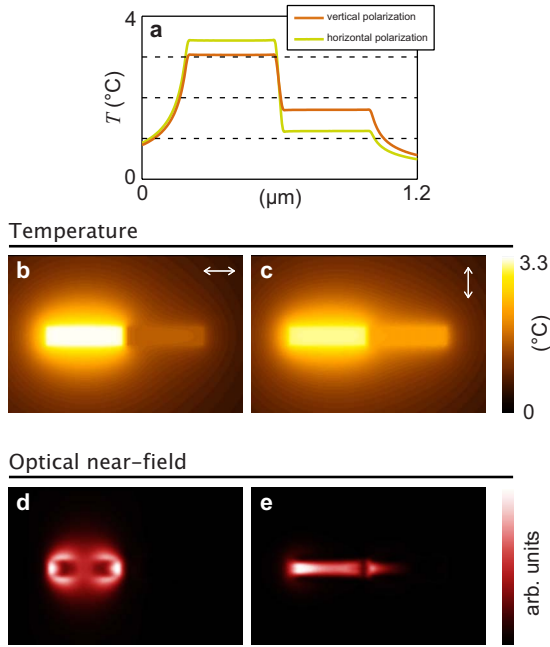
FIG. 9. (Color online) The system consists of two rods, 400 nm long, 100 nm wide, and 50 nm thick, separated by a gap of 20 nm. The structure is lying upon a glass substrate and immersed in water. One of the two rod is illuminated at $\lambda = 700$ nm, $P = 1$ mW/μm^2. (a) Temperature profile observed along the structure for the two polarizations. [(b) and (c)] Associated temperature maps. [(d) and (e)] Associated optical near-field distributions.

ing the rules of optical and thermal energy conversion at the nanoscale in plasmonics for arbitrarily complex nanostructures.

2. Multiple structures

When a plasmonic system is just composed of a single plasmonic structure, the plasmonic structure usually features a uniform temperature because of the high thermal conductivity of metals,[6] which is besides a requisite to apply the LMI method and is usually satisfied in plasmonics. This has already been mentioned above.

When a plasmonic system is composed of disconnected structures (such as a dimer), the temperature is still supposed to be uniform in each individual structure, but the temperature is not supposed to be identical from one structure to another. In the previous paragraph, the temperatures of each part of the gap antenna structure were bound to be the same for symmetry reasons (symmetry regarding both the structure morphology and the illumination conditions). It is the reason why the LMI method could be applied straightforwardly, but when the temperatures are not supposed to be identical, the LMI method as described above no longer applies.

In this paragraph, we explain how the LMI method can be further extended to investigate composite structures in which the temperatures of each structure are not supposed to be identical. For the sake of simplicity, we shall consider a plasmonic system composed of two disjointed structures (Fig. 9) labeled 1 and 2 even though the LMI method can be extended to an arbitrary high number of disjointed structures.

Let N_1 and N_2 be the number of cells of the two structures and T_1 and T_2 their steady-state inner temperatures. In this situation, the matricial Eq. (30) should no longer involve a uniform temperature vector $(T_0)_{i \in [1,N]}$ but a vector in which appear two temperatures: T_1 and T_2. We shall recast Eq. (30) into a matricial formulation to clarify the procedure

$$\begin{pmatrix} \mathbf{e}_1^2 \\ \vdots \\ \mathbf{e}_{N_1}^2 \\ \mathbf{e}_{N_1+1}^2 \\ \vdots \\ \mathbf{e}_{N_1+N_2}^2 \end{pmatrix} = \frac{4\pi\kappa}{\omega v \ \mathrm{Im}(\varepsilon)} \mathbb{A}^{-1} \cdot \begin{pmatrix} T_1 \\ \vdots \\ T_1 \\ T_2 \\ \vdots \\ T_2 \end{pmatrix}. \quad (35)$$

In order to compute the two steady-state temperatures T_1 and T_2, two new energy conservation laws [cf. Eq. (31)] have to be formulated

$$\sum_{i=1}^{N_1} \mathbf{e}_i^2 = \sum_{i=1}^{N_1} |\mathbf{E}_i|^2 \equiv c_1, \quad (36)$$

$$\sum_{i=N_1+1}^{N_1+N_2} \mathbf{e}_i^2 = \sum_{i=N_1+1}^{N_1+N_2} |\mathbf{E}_i|^2 \equiv c_2. \quad (37)$$

The two temperature T_1 and T_2 can now be retrieved from these two coupled equations

$$c_1 = (r_1 T_1 + r_{12} T_2) \frac{4\pi\kappa}{\omega v \ \mathrm{Im}(\varepsilon)}, \quad (38)$$

$$c_2 = (r_{21} T_1 + r_2 T_2) \frac{4\pi\kappa}{\omega v \ \mathrm{Im}(\varepsilon)}, \quad (39)$$

where r_1 and r_2 are the Laplace radii defined by Eq. (33) and r_{12} and r_{21} are coupled radius terms defined as

$$r_{12} = r_{21} = \sum_{i=1}^{N_1} \sum_{j=N_1+1}^{N_1+N_2} (\mathbb{A}^{-1})_{ij} \quad (40)$$

$r_{12} = r_{21}$ since matrix $\mathbb{A}$ is symmetric. These coupled effective radii are negative and can be seen as the sum of the terms of the upper right (or lower left) quadrant of the matrix $\mathbb{A}^{-1}$.

As an example, Fig. 9 presents the results for a gap nanoantenna. The structure is symmetric but the illumination consists of a focused beam that illuminates only one rod. In each rod, the temperature is uniform while a high-temperature gradient is observed in the gap region.

III. CONCLUSION

We have shown how the DDA and the GDT techniques can be further extended to compute the temperature profile in and out plasmonic structures under illumination. Problems involving numerous spherical nanoparticles or complex plasmonic nanostructures lying upon a substrate can be straightforwardly resolved. In the GDT case, the core of the thermal extension relies on a different formalism that we named
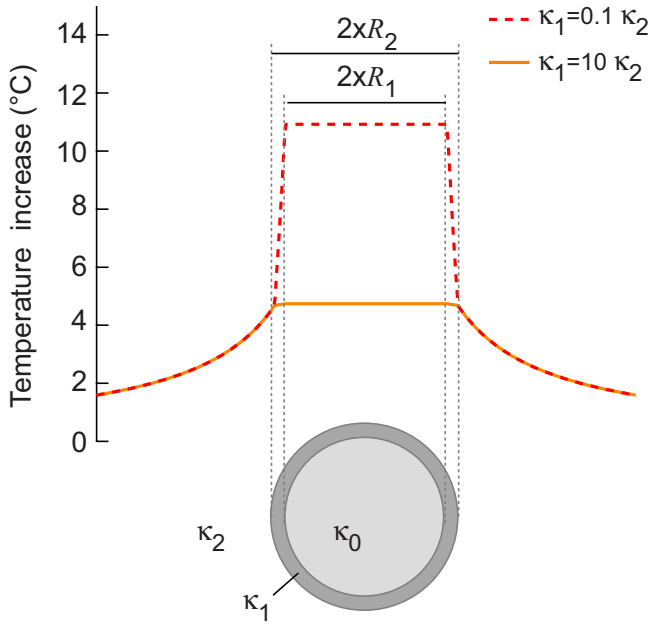
FIG. 10. (Color online) Temperature profile through a sphere of conductivity κ_0 and radius R_1 having a surrounding coating of conductivity κ_1 and thickness R_2-R_1 immersed in a medium of conductivity κ_2. For this example, we chose $Q=1$ μW, $\kappa_0 \gg \kappa_1 = 1$ W/m K, $R_1 = 15$ nm, and $R_2 = 17$ nm. As shown by the two temperature profiles, the presence of a resistive coating does not affect the temperature distribution in the surroundings, only the inner particle temperature is modified.

LMI. In particular, such a formalism allows for a computation of the internal temperature of a plasmonic structure only from the knowledge of the absorption cross section, avoiding any calculation of electric field distribution (Fig. 10).

In order to illustrate the high degree of applicability of this numerical framework, several problems have been addressed. First, by considering a chain of nanospheres, we discuss the influence of a substrate and the nature of the surrounding medium in the temperature distribution around plasmonic structures. Then, by considering an array of $N \times N$ particles, we discuss the collective effect that can be observed when heating an assembly of nanoparticles and what the temperature increase is as a function of the size of the illuminated area. As an application of the LMI formalism, we have computed the optical and thermal near fields around a gap nanoantenna for symmetric and asymmetric illuminations. While a dramatic optical near-field enhancement is observed within the gap region, the temperature remains uniform throughout the nanoantenna. This example illustrates that the design of an efficient plasmonic nanosource of light does not follow the same rules as the design as an efficient plasmonic nanosource of heat.

Through its versatility and easy implementation on any DDA or GDT code, this numerical framework stands for a unique tool that will reinforce the development of a new area of nanotechnology that we could name *nanothermics*, the art of shaping and using temperature at the nanoscale.

APPENDIX A: INFLUENCE OF A SURFACE THERMAL RESISTANCE OF THE NANOPARTICLES ON THE TEMPERATURE PROFILE

It was recently reported that the efficiency of heat exchange at a nanoparticle interface can be affected by any molecular coating that acts as a surface thermal resistance.[16] Our approach does not take into account such an effect. However, we show in this paragraph that any interface resistance is not supposed to affect the temperature increase observed in the surrounding for a given heat power Q released by the nanoparticle.

This effect can be demonstrated using a simple spherical model that can be solved analytically. Consider a sphere of radius R_1 and conductivity κ_0 surrounded by a spherical layer of thickness R_2-R_1 and conductivity κ_1 mimicking a molecular coating. κ_2 is the thermal conductivity of the surrounding medium ($r>R_2$). In each medium $j \in \{1,2,3\}$, the temperature reads $T(r)=a_j/r+b_j$. We suppose that $\kappa_0 \gg \kappa_1, \kappa_2$ so that the nanoparticle temperature T_0 is uniform. By writing continuity relations for the temperature T and the thermal current $-\kappa_j \nabla T$, we obtain the temperature profile in each of the three media

$$r \leq R_1 : T_0 = \frac{Q}{4\pi}\left(\frac{1}{\kappa_1 R_1} + \frac{1}{\kappa_2 R_2} - \frac{1}{\kappa_1 R_2}\right),$$

$$R_1 \leq r \leq R_2 : T(r) = \frac{Q}{4\pi}\left(\frac{1}{\kappa_1 r} + \frac{1}{\kappa_2 R_2} - \frac{1}{\kappa_1 R_2}\right),$$

$$r \geq R_2 : T(r) = \frac{Q}{4\pi\kappa_2 r}. \tag{A1}$$

We observe that the temperature in the surrounding medium is indeed only dependent on the power released by the nanoparticle and the thermal conductivity κ_2 of the surrounding medium. It is not dependent on the thermal properties of the nanoparticle, and in particular, the thermal conductivity κ_1 of the molecular coating. This temperature increase in the surroundings is usually the temperature that really matters since responsible of any thermoinduced phenomena. In a more general way, in a multilayer problem, the conductivities of the inner layers do not affect the temperature of the outer ones.

APPENDIX B: INFLUENCE OF A THERMOINDUCED FLUID CONVECTION ON THE TEMPERATURE PROFILE

A local temperature increase in a fluid within a gravity field can give rise to spontaneous Rayleigh-Bénard instability and fluid convection. The Marangoni effect is a famous example.[17] From this consideration, it is worth wondering if the local temperature increase that a plasmonic nanostructure features under illumination can give rise to fluid instability that might affect the temperature profile calculated by our steady-state numerical approach. In this appendix we show that, on the nanoscale, a temperature profile cannot be affected by any thermoinduced fluid convection.

Such a question can be addressed without carrying out sophisticated hydrodynamic simulations. The orders of magnitude can be simply obtained by dimensional analysis of the differential equations governing the problem.

Consider a nanosource of heat that features a typical temperature increase $T_0 = 50$ °C and whose typical size is $L = 500$ nm. Considering a large nanostructure and high temperature is the most favorable case to induce fluid convection. The fluid dynamics is governed by the steady-state Navier-Stokes equation

$$\rho(\mathbf{v}(\mathbf{r}) \cdot \nabla)\mathbf{v}(\mathbf{r}) = \eta \nabla^2 \mathbf{v}(\mathbf{r}) + \mathbf{f}_{\mathrm{th}}(\mathbf{r}), \qquad (\mathrm{B1})$$

where ρ is the fluid mass density, η the dynamic viscosity, $\mathbf{v}(\mathbf{r})$ the fluid velocity, and $\mathbf{f}_{\mathrm{th}}(\mathbf{r})$ the volumetric force due to temperature nonuniformity. This thermal force can be evaluated by the Boussinesq approximation.[22] This approximation accounts for the temperature dependence of the density by adding an external buoyancy force term, which is dependent on the temperature distribution

$$\mathbf{f}_{\mathrm{th}}(\mathbf{r}) = \rho \alpha g T(\mathbf{r}), \qquad (\mathrm{B2})$$

where g is the gravity, α the dilatation coefficient of the fluid, and $T(\mathbf{r})$ the temperature increase. In the Navier-Stokes Eq. (B1), the first term represents the acceleration of a fluid particle along a stream line. This term does not control the physics of temperature-induced fluid convection. The two forces that are in competition are the viscosity force and the thermal force. Hence, they have to be of the same order of magnitude

$$\eta \nabla^2 \mathbf{v}(\mathbf{r}) \sim \rho \alpha g T(\mathbf{r}). \qquad (\mathrm{B3})$$

Let V be the order of magnitude of the velocity in the fluid. We obtain

$$V \sim L^2 \rho \alpha g T_0 / \eta. \qquad (\mathrm{B4})$$

Using $\rho = 10^3$ kg/m^3, $\alpha = 10^{-4}$ K^{-1}, $\eta = 10^{-3}$ Pa s, and $g = 9.8$ m/s^{-2}, we obtain that the typical fluid velocity of the thermal-induced convection is $V \sim 10^{-8}$ m/s^{-1}. This very slow fluid velocity is mainly due to the small length scale of the system. At such a scale, the viscous force is always dominant (in this particular case the Reynolds number is $\mathsf{Re} = 10^{-8}$) and leads to a highly laminar fluid motion.

We shall see now if such a slow fluid convection can distort the temperature profile. In the presence of fluid convection, Poisson Eq. (11) has to be modified

$$\rho c_{\mathrm{p}} \nabla \cdot [T(\mathbf{r})\mathbf{v}(\mathbf{r})] - \kappa \nabla^2 T(\mathbf{r}) = 0, \qquad (\mathrm{B5})$$

where c_{p} is the specific-heat capacity at constant pressure ($c_{\mathrm{p}} = 4.18 \times 10^3$ J/kg K for water). The first term of Eq. (B5) represents heat transport through fluid convection—it is on the order of $\rho c_{\mathrm{p}} T_0 V / L$—while the second term represents heat transport through heat diffusion—on the order of $\rho c_{\mathrm{p}} T_0 V / L$. The ratio of the orders of magnitude of these two terms gives a dimensionless number—called the Rayleigh number[22]—that quantifies the diffusion versus convection effects

$$\mathsf{Ra} = \frac{\alpha g T_0 L^3}{D \nu}, \qquad (\mathrm{B6})$$

where $D \equiv \kappa / \rho c_{\mathrm{p}}$ is the thermal diffusivity of the medium and $\nu \equiv \eta / \rho$ its cinematic viscosity. In water medium, one can write $\mathsf{Ra} = 10 T_{0(\mathrm{K})} L_{(\mathrm{mm})}^3$ as far as the temperature increase T_0 and length scale L are expressed in Kelvin (or degree Celsius) and millimeter respectively. If the Rayleigh number Ra is much lower (respectively, larger) than unity, thermal diffusion is dominant (respectively, negligible) with respect to fluid convection on the establishment of the temperature profile.

In the present case, $\mathsf{Ra} \sim 10^{-7}$. As a consequence, in nanoplasmonics experiments occurring in waterlike medium, the temperature distribution is mainly governed by heat diffusion and not fluid convection. In other words, on the nanoscale the temperature reaches its steady state distribution so fast that such a slow fluid motion ($V \sim 10^{-8}$ m/s) cannot distort it. This conclusion justifies the use of the standard Poisson equation for the thermal calculations performed within the paper.

*Corresponding author: guillaume.baffou@fresnel.fr

[1] A. O. Govorov and H. H. Richardson, Nano Today **2**, 30 (2007).

[2] S. Link and M. A. El-Sayed, Int. Rev. Phys. Chem. **19**, 409 (2000).

[3] D. Pissuwan, S. M. Valenzuela, and M. B. Cortie, Trends Biotechnol. **24**, 62 (2006).

[4] L. Cao, D. Barsic, A. Guichard, and M. Brongersma, Nano Lett. **7**, 3523 (2007).

[5] E. Rousseau, A. Siria, G. Jourdan, S. Volz, F. Comin, J. Chevrier, and J. J. Greffet, Nat. Photonics **3**, 514 (2009).

[6] G. Baffou, R. Quidant, and J. F. García de Abajo, ACS Nano **4**, 709 (2010).

[7] G. Baffou, R. Quidant, and C. Girard, Appl. Phys. Lett. **94**, 153109 (2009).

[8] S. Berciaud, L. Cognet, G. A. Blab, and B. Lounis, Phys. Rev. Lett. **93**, 257402 (2004).

[9] G. Baffou, C. Girard, and R. Quidant, Phys. Rev. Lett. **104**, 136805 (2010).

[10] G. Baffou, M. P. Kreuzer, F. Kulzer, and R. Quidant, Opt. Express **17**, 3291 (2009).

[11] C. Girard, Rep. Prog. Phys. **68**, 1883 (2005).

[12] M. A. Yurkin and A. G. Hoekstra, J. Quant. Spectrosc. Radiat. Transf. **106**, 558 (2007).

[13] S. Link and M. A. El-Sayed, J. Phys. Chem. B **103**, 8410 (1999).

[14] J. H. Hodak, A. Henglein, and G. V. Hartland, J. Chem. Phys. **112**, 5942 (2000).

[15] C. Girard, E. Dujardin, G. Baffou, and R. Quidant, New J. Phys. **10**, 105016 (2008).

[16] J. Alper and K. Hamad-Schifferli, Langmuir **26**, 3786 (2010).

[17] L. E. Scriven and C. V. Sternling, Nature (London) **187**, 186 (1960).

[18] J. D. Jackson, Classical Electrodynamics (Wiley, New York,

1999).

[19] H. H. Richardson, M. T. Carlson, P. J. Tandler, P. Hernandez, and A. O. Govorov, Nano Lett. **9**, 1139 (2009).

[20] P. Ghenuche, S. Cherukulappurath, T. H. Taminiau, N. F. van Hulst, and R. Quidant, Phys. Rev. Lett. **101**, 116805 (2008).

[21] M. Righini, P. Ghenuche, S. Cherukulappurath, V. Myroshny-chenki, J. F. García de Abajo, and R. Quidant, Nano Lett. **9**, 3387 (2009).

[22] E. Guyon, J. P. Hulin, L. Petit, and C. D. Mitescu, *Physical Hydrodynamics* (Oxford University Press, USA, 2001).